

# Frequency Throttling Side-Channel Attack

Chen Liu<sup>†</sup>, Abhishek Chakraborty<sup>†</sup>, Nikhil Chawla<sup>†</sup>, Neer Roggel<sup>‡</sup>

<sup>†</sup> Intel Corporation, Hillsboro, OR, USA    <sup>‡</sup> Intel Corporation, Rio Rancho, NM, USA  
{chen1.liu,abhishek1.chakraborty,nikhil.chawla,neer.roggel}@intel.com

## ABSTRACT

Modern processors dynamically control their operating frequency to optimize resource utilization, maximize energy savings, and to conform to system-defined constraints. If, during the execution of a software workload, the running average of any electrical or thermal parameter exceeds its corresponding predefined threshold value, the power management architecture will *reactively* adjust CPU frequency to ensure safe operating conditions. In this paper, we demonstrate how such power management-based CPU throttling activity forms a source of timing side-channel information leakage, which can be exploited by an attacker to infer secret data from a constant-cycle victim workload. We highlight the fact that a constant-cycle implementation of code does not necessarily guarantee its constant execution on different data inputs with respect to wall clock time. This is because existing throttling mechanisms perform data-dependent frequency adjustments, which in turn make the running time of the code also data-dependent. The proposed frequency throttling side-channel analysis attack can be launched by kernel-space attackers and user-space attackers, thus compromising security guarantees provided by isolation boundaries. We validate our attack methodology across different systems by performing experiments on a constant-cycle implementation of the AES-128 algorithm. The results of our experimental evaluations demonstrate how the attacker can successfully recover the targeted AES key by correlating the collected timing side-channel traces with the corresponding timing estimates for different key guesses, under frequency throttling. Finally, we discuss different options to mitigate the threat posed by frequency throttling side-channel attacks, as well as their advantages and disadvantages.

## KEYWORDS

Power Management, Frequency Throttling, Side-Channel Analysis

### ACM Reference format:

Chen Liu<sup>†</sup>, Abhishek Chakraborty<sup>†</sup>, Nikhil Chawla<sup>†</sup>, Neer Roggel<sup>‡</sup>. 2022. Frequency Throttling Side-Channel Attack. In *Proceedings of xxx, xxx (xxx)*, 14 pages.  
<https://doi.org/10.1145/nmnmnmnm.nmnmnmnm>

## 1 INTRODUCTION

Power management architectures of modern processor designs play a central role in optimizing for and balancing between high performance and low power consumption requirements, a product of decades of academic and industry innovation [13, 22, 24, 31, 46, 51]. For example, a widely-used power management architectural mechanism known as Dynamic Voltage and Frequency Scaling (DVFS) is available on Intel, AMD and ARM CPUs [36, 38]. DVFS dynamically adjusts CPU frequency and voltage in order to reduce system power

consumption, yielding higher performance per Watt, or to quickly alter CPU frequency during workload execution, in order to ensure that different electrical and thermal parameters of the system remain below predefined safe limits [6, 9, 31]. Similar such throttling has been recently identified as enabling covert channels [25], given its reliance on shared infrastructure across security domains. In this work, we investigate if such workload-dependent CPU frequency adjustments yield exploitable side-channels.

Modern systems also provide multiple software-accessible telemetries which allow users to characterize bottlenecks at scale [11], monitor resource utilization, power and performance [15, 18, 47], and gain insights into system reliability [26]. Recently, researchers have demonstrated how a processor’s energy telemetry reporting framework can be used maliciously to perform power side-channel analysis attacks [40, 41]. These attacks allow a user-space attacker (having Ring 3 privilege) to infer secret information from a targeted victim workload running inside a TEE. In order to thwart such side-channel attacks, CPU vendors (both Intel and AMD) have provided security patches [5, 28] which remove Ring 3 software access to the energy telemetry data via the Linux kernel module. In addition, Intel has also provided a filtering-based mitigation patch [29] to safeguard the reported energy telemetry readings even from a kernel-space attacker (having Ring 0 privilege).

In this paper, we study the potential threat posed by a new type of side-channel information leakage source termed the *frequency throttling side-channel*. Such a side-channel arises due to the dynamic adjustment of CPU frequency when workload execution causes one or more electrical or thermal system parameters to exceed predefined limits. Typically, in such a scenario, the power management architecture throttles CPU frequency to a lower value, for ensuring safe operating conditions of the system. Then, depending on the running average of the parameter(s) in question, CPU frequency is again boosted to a higher value until any limit threshold is violated. Therefore, increases and decreases in CPU frequency (hereinafter, referred to as *average throttling frequency*) during workload execution are dependent on the instantaneous electrical and thermal parameters being capped by system-defined limits. The average throttled frequency in turn affects the overall execution time of the workload, even if its implementation follows constant cycle coding principles [27], or it is being executed inside a TEE. The objective of a side-channel attacker is to deduce the targeted secret from a victim workload by monitoring fluctuations in its execution time for processing different inputs. Unlike software-accessible telemetries, frequency throttling side-channel leakage cannot be thwarted by enforcing access restriction or filtering-based mitigation patches. This is because any presumed malicious Ring 3 software can precisely monitor the execution time of a targeted process by reading timestamp counter values (e.g., using RDTSC [44]).

In this work, we mainly consider the running average power limit (RAPL) controlled CPU frequency throttling activity, demonstrating the feasibility of a throttling side-channel attack. Yet, a similar attack methodology may be equally applicable in scenarios where dynamic CPU frequency adjustments are performed due to other electrical or thermal system constraints. In particular, we focus on the data-correlated power consumption behavior of victim code as considered previously in the *Platypus* attack[40]. While the *Platypus* attack relies on power consumption information directly exposed to privileged software through a telemetry interface, a throttling side-channel *converts* the power differences to power limit-induced execution time differences, which are easily accessible by unprivileged software. It is to be further noted that the *Platypus* attack and the proposed throttling side-channel attack are two different attacks that exploit the same information leakage source, namely data-correlated power consumption resulting from inherent CMOS circuit properties. Also, both attacks require neither physical access to the target platform nor any additional high-precision power measurement setup as required in *traditional* side-channel attacks.

We demonstrate the applicability of the throttling side-channel analysis attack to retrieve secret information from cryptographic primitives by considering an AES-NI-based AES implementation as a case study. The results of our experimental evaluations reveal the effectiveness of such an attack in finding the secret AES key, by performing statistical analysis on the collected timing side-channel traces. In addition, we also discuss potential mitigation options which can be incorporated by cryptographic implementations to thwart throttling side-channel attacks.

The main contributions of this paper can be summarized as follows:

- Presentation of a new type of side-channel attack which exploits the workload-dependent CPU frequency adjustments performed by the power management architecture of modern processors
- Detailed experimental evaluation of the frequency throttling side-channel analysis attack, showing extraction of cryptographic secrets (e.g., AES key) across different systems
- Enumerating necessary conditions of a frequency throttling side-channel attack and providing mitigation options thwarting each of the necessary conditions

The rest of the paper is organized as follows: Section 2 presents background information of power management algorithms and related side-channel attacks. Section 3 presents details related to the source of the throttling side-channel leakage and also, provides an overview of how an attacker can exploit such leaked information. Section 4 describes the threat model and showcases an attack using the throttling side-channel against an AES-NI-based cryptographic implementation. Section 5 discusses different options to mitigate a frequency throttling side-channel. Section 6 discusses possible directions for future work. Section 7 concludes the paper.

## 2 BACKGROUND

### 2.1 Power Telemetry Side-Channel Leakage

*2.1.1 Related Work.* Existing work in related literature has demonstrated the vulnerability of software-accessible energy and power telemetry information to side-channel analysis attacks. In [55], the authors highlighted the use of software-accessible battery data of

an Android phone to extract sensitive information from multiple applications. It has been shown in [19] that energy meter readings can be used to infer control flow dependency as well as cache hit/miss patterns for a program. [43] demonstrated the utilization of energy meter readings to distinguish keys of different Hamming weights for an RSA implementation.

In addition to the above, a couple of recent works have targeted a processor’s energy consumption information (as exposed by Running Average Power Limit (RAPL) interfaces in both Intel and AMD processors) to perform side-channel analysis attacks. In [40], the authors demonstrate software-based power side-channel attacks called *Platypus* to extract a key from a secure enclave, to break kernel address space layout randomization (KASLR), and to establish a timing-independent covert channel. In [41], the authors present a methodology to perform side-channel risk assessment of different software-accessible telemetries including RAPL energy, CPU frequency, voltage, and temperature data.

*2.1.2 Correlation Power Analysis (CPA).* Power analysis attacks exploit the fact that the dynamic power consumption  $P_{dyn}$  of a digital CMOS-based circuit is data-dependent in nature [37], as evident in the following equation:

$$P_{dyn} = \alpha \cdot C \cdot V_{DD}^2 \cdot f \quad (1)$$

where,  $\alpha$ ,  $C$ ,  $V_{DD}$ , and  $f$  represent switching activity factor, load capacitance, supply voltage, and clock frequency, respectively. The main objective of a power side-channel analysis attack is to retrieve a targeted secret by analyzing the data-dependent power consumption of a cryptographic implementation during a selected time window. Traditional physical side-channel analysis techniques such as Correlation Power Analysis (CPA) perform statistical analysis on a large number of side-channel traces which are collected by varying the input data [42]. In a typical CPA attack, the attacker correlates the actual power consumption values  $P_a$  from the collected power traces with the corresponding hypothetical power leakage values  $P_h$  (as calculated using standard Hamming weight or Hamming distance power models). This is done for different key guesses using the following measure:

$$\rho^k = \frac{cov(P_a, P_h^k)}{\sigma_{P_a} \sigma_{P_h^k}} \quad (2)$$

where,  $\rho^k$ ,  $\sigma_{P_a}$ , and  $\sigma_{P_h^k}$ , represent the Pearson’s correlation coefficient for key guess  $k$ , the standard deviation of the actual power values  $P_a$ , and the standard deviation of the hypothetical power values  $P_h^k$  for key guess  $k$ , respectively.

The variation in power consumption values due to processing of different data as measured by existing CPU telemetry interfaces (low sampling rates) is much less pronounced when compared to the variations as captured by traditional physical side-channel setups (high sampling rates). In addition, measurement inaccuracy and noise in the telemetry readings further reduce the signal-to-noise ratio (SNR) of the collected side-channel traces. However, even in spite of these challenges, it has been demonstrated in [40] that the CPA attack is powerful enough to distinguish minute secret-dependent biases in the telemetry readings and thus, can successfully recover the underlying secret data. In this work, we also use a variation of

CPA attack (details in Section 3.1.2) to perform statistical analysis of collected telemetry traces.

**2.1.3 Existing Countermeasures.** A number of possible countermeasures to thwart power telemetry attacks were listed in [40]. These mitigation strategies include restricting user-space access (Ring-3 privilege) to *powercap* driver in Linux and limiting the measurement resolution of telemetry interfaces. In response to the *Platypus* attack, CPU vendors (both Intel and AMD) have updated the Linux *powercap* driver to restrict unprivileged access to RAPL interface [5, 28]. In addition, Intel also issued a mitigation adding white noise to reported RAPL interface readings, which is enforced when Intel SGX is enabled and can be enabled by software via a software switch [29]. These approaches effectively thwart the CPA attack on software-accessible power telemetry data.

## 2.2 CPU Power Management

In this work, we demonstrate how an attacker can leverage the fast dynamic changes in a processor’s *power performance states*, triggered due to its power management-related limits (hereinafter, referred to as *power limits*) to create a novel source of timing side-channel leakage during workload execution. We show that the attack is possible even with the abovementioned countermeasures against power telemetry side-channels, which are not designed to mitigate a frequency throttling side-channel. Here we introduce relevant background information of modern CPU power management, using Intel processors as an example.

**2.2.1 Processor Performance States.** Intel processors implement performance states (referred to as *P-States*, defined per ACPI [16]), by realizing a DVFS mechanism for optimizing power consumption. Such *P-States* correspond to different *voltage-frequency* pairs, which can be **proactively** controlled either by the operating system (using *SpeedStep* [33]) or by the hardware (using *Speed Shift* [34]). As per convention, the highest CPU *P-State* is referred to as P0 and it corresponds to the highest achievable operating frequency, as determined during manufacturing, enabling the processor to enter the so called *turbo mode*.

During execution of a workload, if any system-specific limit (electrical or thermal) is violated, the processor *P-State* is **reactively** controlled by the power management algorithm. The remainder of the paper focuses on reactive limits, which induce the frequency throttling side-channel. Depending on the criticality of the limit being hit, reactive control of *P-States* may be performed with various response times (in the order of a few ms to tens of seconds) to promptly bring the system back to safe operating conditions.

**2.2.2 P-State Control under Reactive Limits.** The power management algorithm of a CPU periodically calculates different running averages of electrical parameters (e.g., power, current, etc.) of windows of pre-specified lengths. The running averages are then compared against respective reactive limit values to compute the power budget, which is the difference between the reactive limit and average consumed power, for example. Based on the power budget, the power management algorithm  $PL\_ALG(\cdot)$  computes the new *P-State* limit  $f_{max}$ , which is the maximum possible CPU

operating frequency that satisfies all the reactive limits of the system. An overview of the new *P-State* upper bound selection process by the controller is presented in Algorithm 1.

When none of the reactive limits are hit, all power budgets remain positive and CPU operating frequency is not capped by  $f_{max}$  (or in other words,  $f_{max}$  is higher than maximum turbo frequency). If any of these calculated running averages exceed a specific reactive limit (e.g., power limit  $PL$ ), the power management algorithm will trigger CPU throttling activity and reduce  $f_{max}$ . In such cases, in order to maximize performance while satisfying the reactive limits, the processor may run at the frequency limit  $f_{max}$ , as governed by its feedback control mechanisms [10].

---

### Algorithm 1 Determination of new *P-State* limit

---

**Input:**

- 1: (i) System reactive limit  $PL_i$  with running average time window  $\tau_i, i \in [1, N]$
- 2: (ii) Polling interval  $T$
- 3: (iii) Current *P-State* limit  $f_{max}$
- 4: (iv) Power management control algorithm  $PL\_ALG(\cdot)$

**Output:** New *P-State* limit  $f_{max}$

```

5: for every  $T$  time units do
6:   for  $i$  from 1 to  $N$  do
7:      $\bar{P}_i \leftarrow$  Calculate avg. power over  $\tau_i$ 
8:      $\Delta \leftarrow \bar{P}_i - PL_i$  /*Available power budget*/
9:      $f_{max,i} \leftarrow PL\_ALG(\Delta)$ 
10:    if  $f_{max} > f_{max,i}$  then
11:       $f_{max} = f_{max,i}$  /*Throttling activity*/
12:    end if
13:  end for
14: end for

```

---

**2.2.3 Common Reactive Limits.** We describe a couple of the *reactive limits* presented in several modern Intel processors [31]. Note that similar reactive limits are also present in the processors of other vendors (e.g., AMD [6], ARM [9]).

- **Running Average Power Limit (RAPL):** RAPL is a feature supported by Intel power management architecture to cap the power consumption on the system. When the configured power limit is exceeded, the CPU will be forced to run at a lower frequency to maximize performance while meeting the power limit requirement. Intel currently provides multiple power limit capabilities, such as package-level power limits (PL1, PL2, PL3) and platform-level power limits (Psys). Ring 0 software can configure the running average window  $\tau$  and the power limit of each capability through MSRs (e.g.,  $MSR\_PKG\_POWER\_LIMIT$  for package-level power limits).
- **Voltage Regulator Thermal Design Current Limit (VR TDC):** VR TDC is a power management feature supported by Intel power management architecture. It is a current limit specified in Amperes, that is maintained in order to satisfy the electrical constraints of the VR. Generally, the algorithm monitors the running average current in Amperes by reading the VR current sensor with the configured time window. If the limit is hit, the processor will engage its frequency throttling to reduce its frequency, in order to ensure current remains within the limit and budget.

## 2.3 Traditional Timing Side-Channel Mitigations

In *traditional* timing side-channel analysis, an attacker exploits differences in execution cycles of victim code to deduce the targeted *secret*. Such timing differences can arise due to data-dependent execution cycles of the victim process or due to mutual access of shared system resources (e.g., cache lines, branch predictors, etc.) by the victim and attacker processes.

Several countermeasures have been proposed in related literature, which use constant-cycle coding principles to address the issue of *traditional* timing side-channel leakage [27]. A short summary of such coding principles is as follows:

- Ensure code processes secret data consistently (i.e., requires same number of clock cycles irrespective of secret data values).
- Ensure secret data values (or values derived from secret data) do not affect the sequence of instructions executed due to a conditional branch or an indirect branch target in the code.
- Ensure memory access patterns (or the data size of load/store operations) are invariant with respect to secret data.

Existing work largely assumes that traditional timing side-channel leakage can be mitigated by applying these principles to the secret data-dependent portions of the code.

## 3 FREQUENCY THROTTLING SIDE-CHANNEL

In this work, we demonstrate that mere application of constant-cycle coding principles is insufficient to thwart timing side-channel attacks, as system clock frequency may vary during the code execution phase and may be data-dependent and leak information.

### 3.1 Attack Primitives

**3.1.1 Source of Throttling Side-Channel.** In modern processors, a major source of throttling side-channel information leakage is related to the workload-dependent reactive control of *P-States* (line 11 of Algorithm 1). Let us consider the example presented in Fig. 1 to understand the underlying implementation details leading to such throttling side-channel leakage. Suppose that the workload under execution is a constant-cycle implementation of a function, *foo* (*arg data*), with input argument *data*. As noted in section 2.3, such a constant-cycle implementation has no traditional timing side-channel leakage. However, as illustrated in Fig. 1(a), the power consumption of the workload due to processing different data inputs (*data*<sub>1</sub> and *data*<sub>2</sub>) might vary due to the differences in internal data-dependent computations of the *foo* function. Without any loss of generality, let us assume that the processing of *data*<sub>1</sub> consumes higher power (*P*<sub>1</sub>) compared to that of *data*<sub>2</sub> (*P*<sub>2</sub>) (i.e., *P*<sub>1</sub> > *P*<sub>2</sub>). If both *P*<sub>1</sub> and *P*<sub>2</sub> are below all system-defined reactive limits, there is no throttling activity and system frequency *f*<sub>default</sub> remains the same irrespective of data consumed by *foo*. Therefore, in this case, there is no data-dependent timing side-channel information leakage, as the execution time of the workload is independent of the inputs.

However, when power consumption reaches or crosses the system’s electrical reactive limits (e.g., the limit is configured to a lower value, or a power-hungry stressor code is executed in parallel

with function *foo*) as illustrated using Fig. 1(b), reactive limit induced throttling activity will be triggered, resulting in a change to *P-States*, as shown in Fig. 1(c). Since *P*<sub>1</sub> > *P*<sub>2</sub>, the average throttling frequency *f*<sub>1</sub> for data input *data*<sub>1</sub> will be lower than the average throttling frequency *f*<sub>2</sub> for data input *data*<sub>2</sub> to satisfy the *same* system-defined electrical or thermal limits. Both of these throttling frequencies will be lower than the default system frequency prior to throttling (i.e., *f*<sub>1</sub> < *f*<sub>2</sub> < *f*<sub>default</sub>). *Crucially*, as shown in Fig. 1(c), the execution time of *foo* with frequency *f*<sub>1</sub> is higher compared to its execution time with frequency *f*<sub>2</sub>. Therefore, even though *foo* is a constant-cycle workload implementation, its execution time becomes data-dependent due to such frequency throttling activity. This forms a new type of side-channel information leakage source in modern processors, which we refer to as the **frequency throttling side-channel**.

To visually appreciate the primitive, we design and run a proof-of-concept (PoC) on an Intel Sky Lake system, plotted in Figure 2. The function *foo* we use is composed of 2.8 billion IMUL instructions, which is a cycle-constant instruction. Each IMUL instruction has one operand fixed and the other operand set to either *data*<sub>1</sub> = 0x0 or *data*<sub>2</sub> = 0xAA..AA. In the first run, we configure reactive limits to high values that will not be reached, to prevent throttling from happening, and then execute *foo* with *data*<sub>1</sub> and *data*<sub>2</sub>, measuring aggregated package energy consumption<sup>1</sup> and time elapsed for *foo*. After repeating 100 times, we plot histograms of the average power consumption (calculated from energy dividing by time) and the time elapsed in Figure 2 (a), respectively. As can be observed, the 0xAA case consumes more power than the 0x00 case and the time it takes to execute *foo* for the two operands is identical. The second run duplicates the first run, except for reducing Power Limit 1 (PL1) to 8W and corresponding PL1  $\tau$  to 1s. With this setting, PL1 is hit, and frequency throttling is triggered. As can be seen from Figure 2 (b), power consumption distributions with different data become indistinguishable and both are capped at 8W, which is the power limit. Critically, *foo* now takes a longer time to execute with 0xAA compared to 0x00, while both are slower than the case without throttling. The results confirm that reactive limit induced throttling converts a power side-channel to a timing side-channel.

**3.1.2 Correlation Power Throttling Analysis (CPTA).** An attacker can apply a statistical measure similar to the one shown in equation (2) to exploit the data-dependent throttling behavior of the system during the execution of a victim application. We dub this *Correlation Power Throttling Analysis*, or *CPTA*. The attacker correlates the actual *PL*-induced execution times *T*<sub>δ</sub> of the victim application from the collected telemetry traces with the corresponding hypothetical execution time values *T*<sub>h</sub> for different key guesses using the following measure:

$$\gamma^k = \frac{\text{cov}(T_\delta, T_h^k)}{\sigma_{T_\delta} \sigma_{T_h^k}} \quad (3)$$

<sup>1</sup>As a proof-of-concept to show power differences, this system did not apply Intel’s Platypus mitigation.

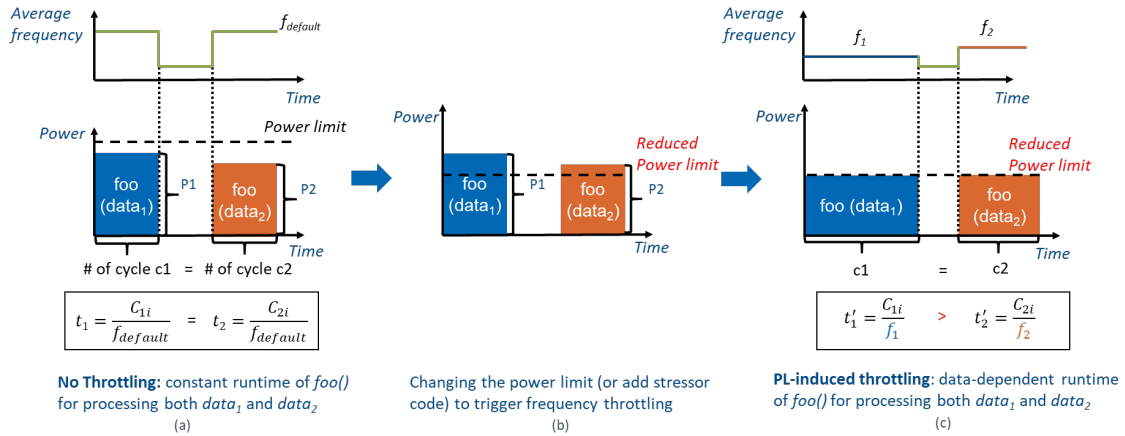


Figure 1: Conversion of power side-channel to timing side-channel leakage by reactive limit-induced throttling.

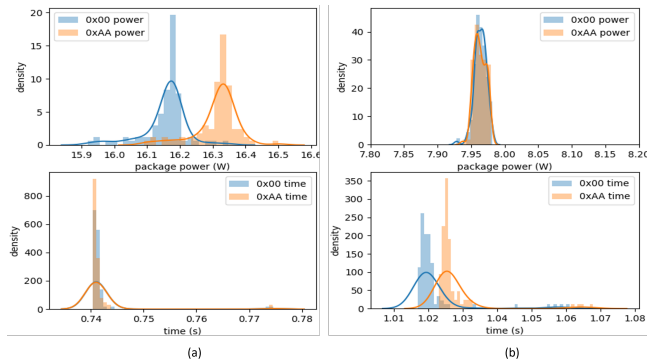


Figure 2: Average power consumption and time elapsed of the same IMUL workload with different operands (a) when throttling is not triggered, and (b) when there is reactive limit induced throttling.

where,  $\gamma^k$ ,  $\sigma_{T_\delta}$ , and  $\sigma_{T_h^k}$ , represent the Pearson's correlation coefficient for key guess  $k$ , the standard deviation of the actual PL-induced execution times  $T_\delta$ , and the standard deviation of the hypothetical execution time values  $T_h^k$  for key guess  $k$ , respectively. Note that such hypothetical execution time values can be modelled similar to the hypothetical power models (see equation (2)) using standard Hamming weight (HW) or Hamming distance (HD) models. This is because the execution time variations due to throttling arises due to the proportional variations in the power consumption values.

### 3.2 Overview of Frequency Throttling Side-Channel Attack

**3.2.1 Threat Model.** We assume the following attack scenarios for an adversary exploiting a frequency throttling side-channel against a victim workload across security boundaries.

- **Attack Scenario 1:** The attacker is a **privileged software attacker** such as kernel-space software or hypervisor. The victim workload is executed inside a Trusted Execution Environment

(TEE), such as Intel SGX [17, 30] or AMD SEV [35, 45, 53]. Such TEEs help protect secret information of the victim application from being directly accessed by even privileged software. In order to enable higher throttling activity during the execution of code residing in a TEE, the attacker can set a lower value of electrical or thermal limit(s) by configuring the corresponding interfaces, such as model-specific registers (MSRs).

- **Attack Scenario 2:** The attacker is a **user-space attacker** with Ring 3 privilege and the victim is another application or the kernel. Unlike the previous scenario, the attacker does not have the privilege to alter the values of the default reactive limits. A Ring 3 attacker instead may execute a stressor code in parallel to the victim code to boost the system power consumption beyond the default limits, such that throttling activity is triggered.

In addition, we assume that the victim code under consideration is implemented using the constant cycle coding principles highlighted in section 2.3. In order to attack such a workload, an attacker utilizes the reactive limit-induced throttling (see section 3.1.1) to make the execution time of the code vary for different *known* data inputs. The main objective of the attacker (for both of the above attack scenarios) is to deduce the targeted secret information of victim code by correlating the secret data-dependent computations with the collected execution time of the code for different data inputs. Note that, in case of a user-space attacker (Attack Scenario 2), the additional noise introduced by the stressor code will degrade the signal-to-noise ratio (SNR) of the collected timing side-channel traces. However, if sufficiently large number of traces are collected to perform statistical analysis (see section 3.1.2), then eventually the Ring 3 attacker will succeed to retrieve the targeted secret of the victim code.

**3.2.2 Attack Methodology.** Fig. 3 presents an overview of the throttling side-channel attack against a constant-cycle implementation of victim workload. Such an attack consists of the following three phases:

- **Offline Phase:** The attacker profiles a victim-like workload with a *known* asset to either configure the related power management settings (Ring 0 attacker) or identify a suitable stressor code (Ring



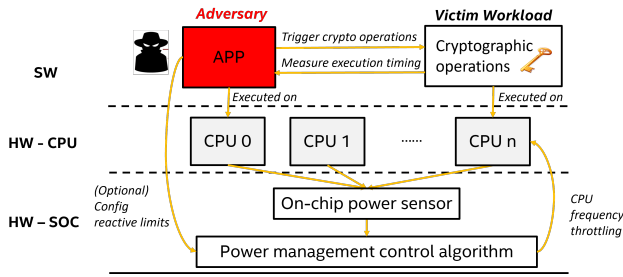


**Figure 3: Exploitation of frequency throttling side-channel information leakage from a victim code.**

3 attacker) such that the victim workload execution will result in triggering of the system’s reactive limits.

- **Online Phase:** The attacker provides different data inputs to the victim code which in turn performs one or more *secret* asset-dependent computations. The attacker also runs a monitor program in parallel to collect the execution time of the victim code for the various different data inputs. If the victim workload execution leads to system throttling activity, such execution time values will exhibit notable variance.
- **Analysis Phase:** The attacker applies analysis methods (such as the CPTA technique, see section 3.1.2) on the collected execution time values, to deduce the targeted *secret* asset of the victim code.

In summary, the above methodology of performing throttling side-channel leakage analysis not only allows an attacker to bypass the security boundary against the victim code, but also enables the attacker to violate the data-invariant execution time guarantees as provided by constant-cycle coding principles.

## 4 CASE STUDY: ATTACK AGAINST AES ENCRYPTION

In this section, we consider a victim workload comprising an AES-NI-based implementation of AES-128 as a case study to illustrate our proposed throttling side-channel attack. Also, we assume the threat model of Attack Scenario 1 as described in section 3.2.1. In order to assess the side-channel leakage due to throttling activity, we use statistical analysis methods derived from *Test Vector Leakage Assessment (TVLA)* [21, 54] and correlation-based analysis (see section 3.1.2).

### 4.1 Victim Workload

**4.1.1 AES-128 Algorithm.** AES is a block cipher established by NIST in 2001 [48]. The algorithm encrypts a fixed size plaintext block of 128-bit using key-size of 128, 192, or 256 bits. The encryption is performed for 10, 12, and 14 rounds for 128, 192, or 256 bits key sizes respectively and the output is a 128-bit ciphertext. The first step in the algorithm is to derive individual round keys using the KeyExpansion procedure [23]. This is followed by the Initial AddRoundKey operation, which computes the bitwise XOR between the plaintext and the round key  $k_0$ . Each subsequent round (except the last round) is composed of four major operations being performed in succession on the intermediate states: SubBytes, ShiftRows, MixColumns, and AddRoundKey. The final round is composed of all the operations except MixColumns. The

baseline AES primitive is extended for encrypting large plaintext blocks using different modes of operation such as ECB, CBC, CFB, OFB, CTR, etc. Optimized implementations of such different AES modes are available as part of Intel’s IPP Crypto library [32]. In this work, we consider the AES-128 primitive to demonstrate its vulnerability to a frequency throttling side-channel attack.

**4.1.2 AES-NI-Based AES Implementation.** AES-NI is an instruction set which improves the AES implementation by accelerating its complex performance-intensive steps using dedicated hardware [23]. In addition to providing enhanced performance compared to software-based AES code, AES-NI instructions also provide improved security against side-channel attacks due to their constant cycle implementations. AES-NI instructions are supported by x86 processors of major vendors, including Intel and AMD.

The AESENC instruction within this set performs a single round of encryption comprising of four operations – ShiftRows, SubBytes, MixColumns and AddRoundKey. The AESENCLAST instruction performs the last round of encryption which excludes the MixColumn operation. Similar to encryption, the set also contains instructions (AESDEC and AESDECLAST) to perform decryption in a constant cycle manner. In this work, we demonstrate the applicability of our proposed throttling side-channel attack against AES by considering the encryption implementation as shown in Algorithm 2. As per the implementation, register %xmm12 initially stores the plaintext while registers %xmm0, %xmm1...%xmm10 store the individual round keys  $k_0, k_1, \dots, k_{10}$  (after KeyExpansion). At the end of the encryption (after AESENCLAST instruction), the ciphertext is stored in %xmm12.

**Algorithm 2** AES-NI-based AES-128 Encryption (AT&T syntax)

```

pxor %xmm0, %xmm12 /*Initial AddRoundKey using k0*/
aesenc %xmm1, %xmm12
aesenc %xmm2, %xmm12
aesenc %xmm3, %xmm12
aesenc %xmm4, %xmm12
aesenc %xmm5, %xmm12
aesenc %xmm6, %xmm12
aesenc %xmm7, %xmm12
aesenc %xmm8, %xmm12
aesenc %xmm9, %xmm12
aesenc %xmm10, %xmm12 /*Last Round using k10*/
    
```

### 4.2 Attack Methodology Details

As outlined in section 3.2.2, the throttling side-channel attack against a victim workload comprises three distinct phases: the offline, the online, and the analysis phases. Next, we present the details of each of these phases as adopted in our case study, using power limit RAPL as an example.

**4.2.1 Offline phase.** During the offline phase, the privileged software attacker first profiles the AES-NI-based victim workload (see Algorithm 2) to estimate  $P$ , which is the power consumption of the victim workload. Then, in order to trigger throttling activity, the attacker adjusts the system’s power limit value  $PL$  such that  $P > PL$ . As per Algorithm 1, such an adjustment will lead to a change in  $P$ -State that satisfies the available power budget. In order to ensure

that there is data-dependent frequency throttling activity, the value of the reactive limit  $PL$  should be carefully adjusted : setting the  $PL$  value too high will not satisfy the requirement of  $P > PL$  whereas setting the  $PL$  value too low will cause the system to execute in a constant low frequency which corresponds to the highest  $P$ -State configuration.

**4.2.2 Online phase.** During the online phase, the attacker inputs plaintext to the victim workload (AES encryption) and obtains the corresponding ciphertext as output. Note that due to PL-induced throttling activity, different plaintexts will have different processing times which correspond to the side-channel traces. During the  $i^{th}$  trace collection, the attacker first records the starting time stamp counter value ( $T_1^i$ ) just before sending the  $i^{th}$  plaintext to the victim workload and subsequently, also records the end time stamp counter value ( $T_2^i$ ) just after receiving the  $i^{th}$  ciphertext. Then, the attacker calculates the corresponding execution time  $T_\delta^i$  by calculating the difference between the time stamp counter values, i.e.,  $T_\delta^i = T_2^i - T_1^i$ . On most of the modern CPUs, incrementing of the time stamp counter is *frequency-invariant* so the  $T_\delta$  captures wall clock time of the victim's execution time and will not be impacted by frequency throttling [7, 31].

**Techniques to reduce Minimum Time to Disclosure:** We define *Minimum Time to Disclosure (MTD)* as the minimum time spent to recover the secret information by collecting side-channel traces. One approach to reduce MTD is increasing Signal-to-Noise (SNR) per trace [42]. We define  $P_v$  as the average power consumption of the victim workload during  $T_\delta$ , where  $T_\delta$  is the execution time of the victim within  $\tau$ . The average power consumption of the rest of the system is defined as  $P_n$ . Then, the *running average power consumption* during  $\tau$  would be  $\bar{P} = \frac{P_v \times T_\delta + P_n \times \tau}{\tau}$ . We can represent the percentage of difference between  $\bar{P}$  and  $P_v$  as follows:

$$\frac{\bar{P} - P_v}{P_v} = \frac{\frac{P_v \times T_\delta + P_n \times \tau}{\tau} - P_v}{P_v} = \frac{T_\delta - \tau}{\tau} + \frac{P_n}{P_v} \quad (4)$$

A better fitting of  $P_v$  with  $\bar{P}$  reduces the above percentage difference to about 0 and thus, diminishing the noise contributing factors (or in other words, improving the SNR). In our experiments, we adopted multiple techniques to achieve this:

- The first technique is to repeatedly execute the victim workload when  $T_\delta$  is shorter than  $\tau$ . In case of the AES-NI workload, the attacker may send  $N$  blocks of the same plaintext for encryption and measure the aggregated execution time as  $T_\delta = N * T_b$ , where  $T_b$  corresponds to the time taken to encrypt one plaintext block. Note that  $T_b$  is typically in the order of tens of ns which is much shorter compared to the reactive limit time window  $\tau$  (which ranges from a few ms to multiple s). However, by selecting a sufficiently large value of  $N$ , the attacker can ensure  $T_\delta$  is approximately equal to  $\tau$ .
- The second technique is to execute multiple instances of the victim workload simultaneously across multiple cores, which results in an increase of its average power consumption  $P_v$ , thus reducing the factor  $\frac{P_n}{P_v}$  in equation (4).

Note that in order to further reduce the *MTD*, the attacker could select the system reactive limit having the lowest possible configurable value of  $\tau$  to trigger throttling activity during execution of

the victim workload. This is because a shorter  $\tau$  implies a smaller value of  $N$  is required to ensure  $T_\delta$  is approximately equal to  $\tau$ . This in turn implies faster trace collection in the online phase, thus reducing the *MTD* for the attack.

**4.2.3 Analysis phase.** We utilize two statistical techniques to analyze potential side-channel information leakage arising from throttling side-channel activity: (i) First, in order to ascertain if different data exhibit different PL-induced throttling behavior, we apply TVLA to the corresponding timing traces. (ii) Second, depending upon the positive outcome of the TVLA, we perform a CPTA attack as described in this section, in order to determine if the targeted AES encryption key can be recovered by analyzing the collected timing side-channel traces. Next, we present the details of these statistical techniques as adopted in our experiments.

**TVLA:** TVLA methodology utilizes t-scores generated from Welch's t-test to assess potential side-channel leakage in cryptographic implementations [20]. In a Welch's t-test, two datasets A and B defined by a statistical measure. *t-score* is computed using  $\mu_1$  and  $\mu_2$  as their sample mean and  $s_1^2, s_2^2$  as their sample variance, shown in equation (5).

$$t\text{-score} = \frac{\mu_1 - \mu_2}{\sqrt{\frac{s_1^2}{N_1} + \frac{s_2^2}{N_2}}} \quad (5)$$

where,  $N_1$  and  $N_2$  are a number of samples in dataset A and B respectively. The null hypothesis of t-test is that the samples from these two sets are drawn from the same distribution, and therefore not distinguishable. A  $|t\text{-score}| > 4.5$  rejects the null hypothesis with 99.999% confidence, indicating the two datasets are statistically distinguishable [52]. In a general TVLA test, two sets of side-channel traces are collected, during encryption of a "Fixed" and a "Random" plaintext with the same key and a t-score is computed for these two sets of traces [20].

In this work, we assess the throttling side-channel leakage of a victim workload (AES-NI-based AES implementation) using the above mentioned TVLA methodology. We applied the TVLA test on the collected timing traces corresponding to encryption of three different sets of plaintexts (*All\_one*, *All\_zero* and *Random*). The configurations of different TVLA tests are as follows:

- **TVLA Test 1:** Dataset A ( $T_\delta^{All\_zero}$ ) comprises of timing traces for encrypting all zero plaintext and dataset B ( $T_\delta^{All\_one}$ ) comprises of timing traces for encrypting all one plaintext.
- **TVLA Test 2:** Dataset A ( $T_\delta^{All\_zero}$ ) comprises of timing traces for encrypting all zero plaintext and dataset B ( $T_\delta^{Random}$ ) comprises of timing traces for encrypting random plaintexts.
- **TVLA Test 3:** Dataset A ( $T_\delta^{All\_one}$ ) comprises of timing traces for encrypting all one plaintext and dataset B ( $T_\delta^{Random}$ ) comprises of timing traces for encrypting random plaintexts.

**CPTA Attack:** In order to perform a CPTA attack, the attacker feeds randomly generated plaintexts to the victim workload and collects PL-induced timing traces  $T_\delta$ . The correlation measure  $\gamma$  (see equation (3)) detects if there is any dependency between  $T_\delta$  and the hypothetical execution time values  $T_h$  to deduce a secret key. In a conventional CPA attack, measured power traces are correlated

with a hypothetical power model based on either HW or HD of targeted intermediate values [14]. Since frequency throttling converts data-dependent correlation in power to execution time, HW/HD models are suitable for computing the hypothetical execution time values.

*Points of Attack:* The attacker targets the following two operations of the victim workload implementation (see Algorithm 2).

- Initial AddRoundKey (PXOR) to find  $k_0$  using HW model.
- Last round (AESENCLAST) to find  $k_{10}$  using HW/HD models.

Once all the bytes of any round key are recovered, InvKeyExpansion procedure can be used to derive the secret AES key [23]. Note that the intermediate AES rounds are typically not considered as attack points because in those cases the corresponding hypothetical execution time values become a function of multiple round keys, thus substantially increasing attack complexity.

---

#### Algorithm 3 AESENCLAST Instruction Code Sequence

---

```

1: aesenclast %xmm10 %xmm12 /* %xmm10 contains  $k_{10}$  */
2:  $Tmp \leftarrow \%xmm12$ 
3:  $RoundKey \leftarrow \%xmm10$ 
4:  $Tmp \leftarrow ShiftRows(Tmp)$ 
5:  $Tmp \leftarrow SubBytes(Tmp)$ 
6:  $\%xmm12 \leftarrow Tmp \oplus RoundKey$ 

```

---

*Execution Time Estimates:* To recover  $k_0$ , the hypothetical execution time values can be modeled using HW of the initial AddRoundKey output as shown in the following equation.

$$T_h^{k'} = HW(p_0 \oplus k'_{0,0}) \quad (6)$$

where,  $T_h^{k'}$  represents the hypothetical execution time values for key guess  $k'_{0,0}$  (corresponding to the first byte of key  $k_0$ ) and  $p_0$  represents the first byte of the plaintext.

In order to understand the execution time value estimates of  $k_{10}$ , let us first look into the details of the AESENCLAST instruction as highlighted in Algorithm 3. Note that the input to the last round (line 1) is stored in register `%xmm12` and in the end the output (ciphertext  $c$ ) is updated in the same register (line 6). Now, the attacker can model the HW-based execution time estimates targeting  $k_{10}$  as follows.

$$T_h^{k'} = HW(ShiftRow^{-1}(SubBytes^{-1}(c_0 \oplus k'_{10,0}))) \quad (7)$$

where,  $T_h^{k'}$  represents the hypothetical execution time values for key guess  $k'_{10,0}$  and  $c_0$  represents the first byte of the ciphertext. Similarly, the attacker can model the HD-based execution time estimates targeting  $k_{10}$  as follows.

$$T_h^{k'} = HD(ShiftRow^{-1}(SubBytes^{-1}(c_0 \oplus k'_{10,0})), c_0) \quad (8)$$

*Attack Outcome:* The CPTA attack utilizes the above mentioned execution time estimates  $T_h^{k'}$  along with the corresponding actual execution time  $T_\delta$  measurements for several plaintexts to compute the correlation measure  $\gamma$  as outlined in equation (3). Subsequently, for each  $j^{th}$  byte of round key  $k_i$  (denoted as  $k_{i,j}$ ), the ranks of all

possible key guesses  $rank(k'_{i,j})$  are sorted in descending order of their correlation measures  $\gamma^{k'_{i,j}}$  as follows.

$$rank(k'_{i,j}) = argsort(\gamma^{k'_{i,j}}) \quad (9)$$

In this work, we define a new metric called Guessing Complexity (GC) to evaluate the success of a CPTA attack. The metric GC is a modified version of the standard *Guessing Entropy* metric [50]. For the  $i^{th}$  round key  $k_i$ ,  $GC_i$  sums the ranks (logarithmically) of correct key byte guesses as shown in the following equation.

$$GC_i = \sum_{j=1}^{16} \log_2[rank(k_{i,j}^{correct\_key})] \quad (10)$$

where,  $rank(k_{i,j}^{correct\_key})$  is the rank corresponding to the correct key byte guess ( $k'_{i,j} = k_{i,j}^{correct\_key}$ ),  $j \in [16]$ . The convergence of the CPTA attack is indicated by the reduction in GC values with the increasing number of timing traces. A value of  $GC = 0$  implies all key bytes have been recovered. In practice, a successful CPTA attack should result in a GC value lower than a pre-defined threshold which allows the recovery of most key bytes with reasonable computational complexity.

### 4.3 Evaluation

In this section, we first report the experimental outcomes of TVLA tests to highlight potential side-channel information leakage arising from frequency throttling activity. Then, we present the results of a CPTA attack to demonstrate how an attacker can successfully recover the secret key by collecting timing side-channel traces of the AES-NI based AES-128 implementation. Our experiments mainly focus on Intel systems, where we consider both power limit-induced and current-limit induced frequency throttling activity during trace collection. Additional experimental results on an AMD processor are also provided in Appendix A.

**4.3.1 Experimental Setup.** We developed a Proof-of-Concept (PoC) code to implement the AES encryption process outlined in Algorithm 2. In our implementation, multiple instances of the encryption (using the same plaintext and key) are executed in parallel across cores for several number of iterations to boost the SNR of the collected timing trace. The number of iterations were calibrated for different systems such that every trace spans approximately 45ms. In our trace dataset, a single trace corresponds to the aggregated execution time of the victim workload (corresponding to the calibrated iteration count) measured using RDTSC. All the experiments are performed in Ubuntu 20.04.

For experimental evaluations, we considered three Intel systems: E3-1230V5 (Sky Lake), i7-1185G7 (Tiger Lake), and Xeon Gold 6326 (Ice Lake). Table 1 lists the details of different systems along with their corresponding power limit (PL2) configurations as adjusted in the offline phase to introduce frequency throttling activity during workload execution. The reason behind selection of PL2 is related to its lowest possible configuration of running average time window of  $\tau=2ms$  among all the power limits available in an Intel system. Note that the lower the  $\tau$  value, the higher the granularity of frequency throttling activity performed by the power management

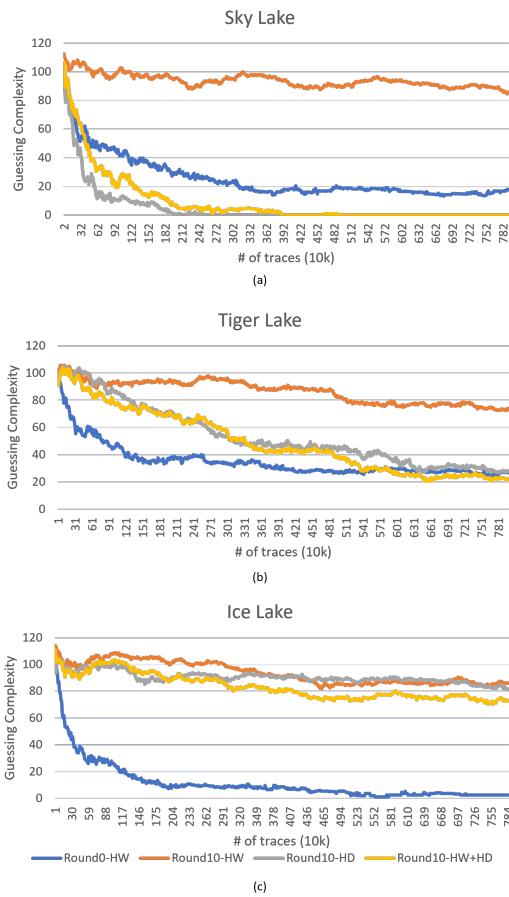


**Table 1: Information and configurations of the systems under test**

Processor Number	Code name	# of physical cores	Max Turbo frequency	SMT	PL2 configuration	PL2 $\tau$
E3-1230V5	Sky Lake	4	3.8 GHz	Disabled	10W	2ms
i7-1185G7	Tiger Lake	2	4.1 GHz	Disabled	8W	2ms
Xeon Gold 6326	Ice Lake	8/socket	3.5 GHz	Disabled	50W	2ms

**Table 2: pairwise t-score (absolute value) among *All\_zero*, *All\_one*, and *Random* traces, repeated on Sky Lake, Tiger Lake, and Ice Lake. T-score greater than 4.5 are marked in red and indicates the set of data are statistically distinguishable.**

	Sky Lake			Tiger Lake			Ice Lake		
	All_zero_2	All_one_2	Random_2	All_zero_2	All_one_2	Random_2	All_zero_2	All_one_2	Random_2
All_zero_1	1.02	<b>41.02</b>	<b>26.20</b>	0.23	<b>10.57</b>	<b>5.32</b>	0.45	<b>19.82</b>	<b>12.51</b>
All_one_1	<b>38.42</b>	2.38	<b>11.79</b>	<b>12.58</b>	3.02	<b>8.08</b>	<b>19.74</b>	0.53	<b>7.57</b>
Random_1	<b>24.07</b>	<b>14.28</b>	2.36	1.32	<b>9.23</b>	3.84	<b>11.27</b>	<b>7.72</b>	0.68

**Figure 4: Guessing Complexity trend with different amount of traces on (a) Sky Lake, (b) Tiger Lake, and (c) Ice Lake systems, with power limit-induced frequency throttling.**

architecture (see Algorithm 1 for details). Also, note that since Xeon Gold 6326 is a 2-socket server system with power limits being defined per socket, we run victim workload on socket 0 by adjusting only PL2 corresponding to socket 0.

**Table 3: Converged Guessing Complexity (GC) with 8M traces. Lower GC implies more key bytes are recovered.**

	Sky Lake	Tiger Lake	Ice Lake
Round0-HW	17.5	27.5	2.6
Round10-HW	85.7	73.3	86.0
Round10-HD	0	27.3	81.2
Round10-HW+HD	0	21.4	72.7

**4.3.2 T-test Results.** For every system under test, following the TVLA methodology described in 4.2.3, we collected 10,000 timing traces of the victim workload corresponding to the encryption of each of the plaintext sets (*All\_one\_1*, *All\_zero\_1* and *Random\_1*). We repeated the trace collection process with the *same* plaintext sets (*All\_one\_2*, *All\_zero\_2* and *Random\_2*) in order to ascertain that there are no false positives in the TVLA test outcomes due to issues associated with data collection (e.g., inconsistent system behaviors or settings). Subsequently, we first removed outlier traces followed by calculation of Welch's *t-score* measure using the remaining trace sets which correspond to every possible pairs of plaintext sets. The results of this experiment are presented in Table 2, where the *t-score* values greater than 4.5 are marked in red to indicate that the pairs of datasets are statistically distinguishable. It can be observed that across all the three systems, *t-score* values between trace sets corresponding to different plaintext sets are higher than 4.5 (the only exception being the case *Random\_1* vs. *All\_zero\_2* in Tiger Lake system) while the *t-score* values between trace sets corresponding to same plaintext sets are lower than 4.5. This signifies that due to power limit-induced throttling activity, the CPU frequency changes in a data-dependent manner, which leads even a constant-cycle victim code implementation to exhibit data-dependent runtime differences.

**4.3.3 CPTA Attack Results with Power Limit.** With the TVLA tests exhibiting positive signs of potential side-channel information leakage, we further investigated the applicability of a CPTA attack on the power limit-induced timing traces, to recover the secret AES key. On each of the systems, we collected 8 million timing traces of the PoC code (with a fixed key) by providing randomly generated plaintexts. The trace collection process took about 100 hours on average across different systems. After the trace collection phase,

we computed the median  $\mu$  of the collected traces and discarded the outliers from the dataset by removing the traces which do not belong to the range of  $[0.95\mu, 1.05\mu]$ . Subsequently, we applied the CPTA attack on the filtered trace dataset, targeting the AES rounds keys  $k_0$  and  $k_{10}$ . The execution time estimates of the AES-128 PoC code as used in our analysis include the following:

- **Round0-HW**: HW of AddRoundKey output, see equation (6).
- **Round10-HW**: HW of the last round, see equation (7).
- **Round10-HD**: HD of the last round, see equation (8).
- **Round10-HW+HD**: Sum of equations (7) and (8).

Also, in our experiments we set  $GC_0=GC_{10}=GC=80$  as the pre-defined threshold for both round keys  $k_0$  and  $k_{10}$  to determine the success of the CPTA attack. Note that  $GC=80$  signifies that the computational complexity of a brute force attack to find the round key is reduced to  $2^{80}$ . In Fig. 4, we present the GC trends (corresponding to different execution time estimate models) versus the number of timing traces considered for the CPTA attack across multiple systems. Based on the data, we make the following observations:

- **The general trend** is that GC converges gradually when increasing number of traces are used for analysis. This is because a larger number of traces helps to reduce the effect of noise in the collected traces. Such GC trends highlight the fact that all the execution time estimate models considered correlate with the actual execution times of the PoC code. Also, it can be observed that in all cases, GC values start from somewhere around 112. This is because the expected value of the initial rank of correct key byte (without parsing any side-channel traces) is 128 among the 256 possible key byte guesses. Therefore, the expected value of initial GC value is  $E(GC) = \sum_{i=1}^{16} \log_2(128) = 112$ .
- **Round0-HW model** appears to be effective on all the three systems: GC converges to 17.5 on Sky Lake, 27.5 on Tiger Lake, and 2.6 on Ice Lake. Especially, on Ice Lake, with this execution time estimate model, we successfully recover 14 out of the 16 bytes of the correct key. The ranks of the remaining two key bytes are 2 and 3.
- **Round10-HW model** converges the slowest among all the models tested. On both Sky Lake and Ice Lake systems, even after analyzing with 8M traces the GC values remain above the considered threshold of 80, signifying that the CPTA attack was unsuccessful in these cases. The lowest GC value obtained was 73.3 on Tiger Lake system.
- **Round10-HD model** shows distinctly different behaviors on different systems. On Sky Lake system, for example, GC converges to 0 (all key bytes recovered) with less than 2M traces. Also, on Tiger Lake system, for this model GC converges to 27.3, similar to Round0-HW model. But in case of Ice Lake system, for this model GC value reduces to only 81.2 which is above the considered threshold.
- **Round10-HW+HD model** results in consistently lower GC values compared to the Round10-HW model across all the three systems. However, compared to the Round10-HD model, for this model the GC value converges slower on Sky Lake system whereas the GC values converge faster on Tiger Lake and Ice Lake systems.

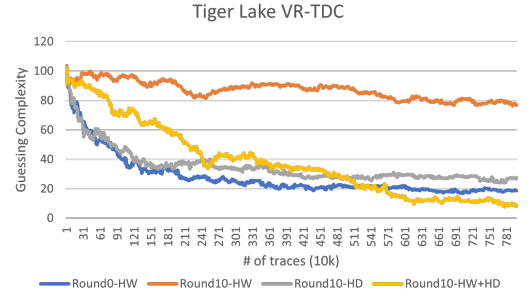


**Figure 5: Guessing Complexity trend with different amount of traces on Tiger Lake, with current limit-induced frequency throttling.**

Note that for a given execution time estimate model, the difference in behavior of GC trends on different systems is likely due to variations in the underlying hardware micro-architecture designs and the fabrication technologies used. Table 3 summarizes the outcomes of the CPTA attack corresponding to different execution time estimate models across systems. These results demonstrate the fact that power-limit induced frequency throttling activity can be successfully leveraged by an attacker to extract secret information from cryptographic workloads.

**4.3.4 CPTA Attack Results with Current Limit.** We also repeated the CPTA test on the Tiger Lake system with VR-TDC limit set to 7 Amperes to trigger frequency throttling. All other configurations were kept the same as used for the power-limit induced frequency throttling experiments in the previous subsection. The GC trends for different execution time estimate models are shown in Figure 5. Similar to the power-limit experiments, the GC value corresponding to the Round10-HW model converges the slowest amongst all the models tested. The GC values for both Round0-HW and Round10-HD models converge to around 20 after analyzing with 8M traces. The GC value corresponding to Round10-HW+HD model converges to the lowest value (around 10) for the CPTA attack with current limit. These observations confirm the fact that VR-TDC limit can also be leveraged by an attacker to mount the frequency throttling side-channel attack.

## 5 MITIGATION

In this section, we discuss different countermeasures to safeguard a victim workload from being susceptible to frequency throttling side-channel attacks. Before going to the details of the mitigation strategies, we first summarize the conditions that must be satisfied to mount such an attack.

- **Condition 1 (Secret Dependency):** The victim code processes a secret asset that is vulnerable to a power side-channel attack. This requires (i) the victim software implementation to be vulnerable to *traditional* physical side-channel attacks and (ii) the underlying hardware system to exhibit variation in power consumption profiles for processing different data.
- **Condition 2 (Controller Actuation):** One of the reactive limits of the system is being hit during victim code execution. This

will cause the power management architecture to trigger frequency throttling activity based on the available power budget (see Algorithm 1 for details).

- **Condition 3 (Observability):** The attacker can monitor the execution time (wall clock time) of the victim code with sufficiently high resolution, or else an equivalent quantity.

In order to thwart side-channel information leakage due to frequency throttling activity, the designer should consider targeting the above mentioned necessary conditions of the exploit. Next, we present different potential countermeasures along with their respective advantages and disadvantages.

## 5.1 Analysis of Secret Dependency

*5.1.1 Necessary conditions of Secret Dependency.* Since power side-channel is the fundamental root cause of power management throttling side-channel, the necessary conditions for the physical power side-channel attack also need to be satisfied for throttling side-channel (except for the physical access capability to measure power). First, the victim application needs to process a secret asset (e.g., cryptographic key) with a confidentiality requirement. Second, power consumption of the underlying hardware processing the secret is correlated with the asset. Third, the implementation of the victim application is susceptible to side-channel attack. For example, the victim application provides the capability for the adversary to repeatedly initiate cryptographic operations with the same sensitive key to collect enough data. Also, for block ciphers, the adversary should have the ability to read input/output or inter-round state of the block cipher primitives. Please note that the input/output is not necessarily the plaintext or ciphertext. One example is the counter (CTR) mode of operation for block ciphers, where the input to the block cipher is the concatenation of the nonce and counter instead of a plaintext.

*5.1.2 Mitigations.* Most of the existing countermeasures against traditional power side-channel will be as effective against a frequency throttling side-channel. For example, software-based masking [49] that splits a secret asset into multiple random shares will randomize the power consumption of the hardware, and will be useful against a frequency throttling side-channel. There are several noteworthy exceptions. For example, shuffling-based countermeasures that randomize instruction execution order, while being effective in making trace alignment and identification of points of interest harder for physical power side-channel attacks, are less effective in mitigating a frequency throttling side-channel. This is because reordering instructions at the cycle granularity is less likely to impact average power consumption during the averaging time window of milliseconds or longer. Also, since an adversary does not need to physically access the hardware, any protection that physically isolates the system will not be sufficient to prevent a frequency throttling side-channel attack.

For cryptographic applications based on existing cryptographic libraries, an example of a generic countermeasure against power side-channel is *key refresh*. One of the necessary conditions for power side-channel is *amplification*, or the ability to repeatedly kick off cryptographic operations with the same sensitive key to collect a sufficient amount of traces. If the secret key is refreshed before enough traces can be collected, it will be harder for the attacker

to fully deduce the secret. One important design factor is the key refresh frequency, which may be based on timing (e.g., refresh per several hours) or data volume (e.g., the volume of data being encrypted with the same key). If the implementer is uncertain of the threshold to use, the lowest threshold that meets performance and design requirements should be selected. Naturally, the practicality of key refresh depends on the specific cryptographic use case (e.g., key refresh is typically not applicable to disk encryption).

From a hardware perspective, secret dependency is satisfied for almost all modern CPUs since power consumption differences due to circuit switching behavior are an inherent property of CMOS circuits. Making the entire SoC power-constant would of course address this condition, but is difficult to achieve. A more feasible option is making specific security-sensitive hardware components (e.g., hardware cryptography accelerator) power-constant.

## 5.2 Analysis of Controller Actuation

This condition allows conversion from power differences to timing differences during an attack. As described in Algorithm 1, the new frequency limit after throttling  $f_{max}$  is a function of the power budget, which is the difference between the power limit  $PL$  and the measured average power consumption  $\bar{P}$ . A mitigation may target one of the components in this conversion process: the control algorithm,  $PL$ , or  $\bar{P}$ .

*5.2.1 Mitigations targeting the control algorithm.* Since the purpose of reactive limits is to restrict a system from consuming power or current beyond the limit while maximizing system performance, a control algorithm is typically designed to select the highest possible frequency limit that satisfies the reactive limits. A straightforward mitigation option to change the control algorithm is to only allow the system to run at the lowest frequency when reactive limits are hit. While it prevents data-dependent frequency change, system performance is severely impacted. Another option is to fully disable reactive limit based throttling, which is usually not acceptable, since it is a critical power management feature widely used. An option to trade-off between security and functionality is to reduce sensitivity of the control algorithm so switching of the frequency limit would be less correlated with the input.

*5.2.2 Mitigations targeting reactive limits.* Similarly, a firmware or system software may take a straightforward approach to either configure the limit to a value too high to hit, or keep it very low so that the system always runs at the lowest frequency. However, these changes have severe negative impact on performance or functionality. One alternative solution is to randomly "fuzz" the reactive limit. For example, instead of configuring a static reactive limit to  $PL$ , firmware or system software may define a range  $[PL_{Low}, PL_{High}]$ , and randomly select a value in the range, dynamically and routinely configuring the reactive limit. By doing so, randomness will be introduced in the power budget, as well as CPU frequency.

As discussed, interfaces (e.g., MSRs) to configure reactive limits, if accessible, could be utilized by an adversary to reduce the limits and trigger the throttling side-channel attack. A cloud service provider (CSP) or system software could prevent these interfaces from being exposed to untrusted guest VMs or ring-3 software, and be aware of the risk if the interfaces have to be exposed.

**Table 4: Summary of mitigations against the frequency throttling side-channel**

#	Mitigation Target	Mitigation Description	Applicable Layer(s)	Mitigation Effectiveness	Perf./Func. Impact
1	Secret Dependency	Existing traditional power side-channel mitigations (e.g., masking, key refresh)	User App/System SW/HW	Vary	Vary
2	Controller Actuation	Keep the system at lowest frequency or disable reactive limits	System SW/HW	Fully	High
3		Reduce sensitivity of throttling control algorithm	HW	Partially	Medium
4		Add randomness to the reactive limit	System SW/HW	Partially	Medium
5		Avoiding exposing reactive limit configuration interfaces to untrusted entities	System SW	Partially	Low
6		Use modelled power instead of actual power in throttling control algorithm	HW	Fully	High
7		Add noise to power input of throttling control algorithm	HW	Partially	Medium
8	Observability	Utilize inherent noise or inject artificial noise to cryptographic operations	User App/System SW	Partially	Medium

*5.2.3 Mitigations targeting average power.* The processor may decouple the calculated average power consumption from the actual power consumption. One approach is to utilize modelled power consumption instead of the actual power reading in the algorithm. If the model is selected to exclude information of instruction operands, then the average power will be independent of any secret data consumed by the victim application. Another approach is for the processor to "fuzz" the average power consumption by adding noise to the value before the control algorithm uses it to compute the power budget. This is equivalent to the idea of fuzzing the reactive limit, since power budget is the difference between reactive limits and the average power. Please note that although fuzzing the power reading will not directly change power consumption, it will alter  $f_{max}$  and indirectly impact power consumption and performance.

### 5.3 Analysis of Observability

One of the common countermeasures against side-channel attacks is to jam the channel with noise to prevent the attacker from deducing the secret. As the side-channel in this attack is frequency and timing information, noise can be injected into the frequency transition or timing information. One method is to leverage inherent noise during cryptographic application calls. As the cryptographic library provider or cryptographic application provider, one may restrict the maximal size allowed of processed data per API invocation, so that more invocations of the API are needed to process the same amount of data, and larger intrinsic noise will be introduced. Besides that, a cryptography implementer may proactively inject random noise to cryptographic operations to increase timing variation. To implement this countermeasure, the developer may add dummy instructions that introduce sufficient power or latency variation. The dummy instructions should be independent of the secret data used in the cryptographic function. For example, timing variation can be introduced using a loop of instructions with random iterations. In addition to that, any power variation induced by the dummy instructions may also increase the entropy of the frequency transition. To ensure randomness is introduced for every frequency transition, it is recommended that some noise is injected during the time window  $\tau$  of the reactive limits that the attacker would target. One possible way to trade-off security and performance impact is to combine this scheme with a key refresh countermeasure, to increase the time needed to perform a successful attack to a key lifetime that is acceptable.

### 5.4 Summary of Mitigation Options

A summary of the mitigations is listed in Table 4, categorized based on the condition to address, the layer(s) to apply, the security effectiveness in mitigating the frequency throttling side-channel, and the performance or functional impact. As can be seen, options that fully resolve the security issue (e.g., #2 and #6) bring high performance or functional impact, while options that partially reduce the security risk have low to medium impact. Depending on the layer in which the mitigation is applied, different options might be selected. For example, the developer of a user-space cryptography implementation may consider options #1 and #8, which are the options available to ring-3 software.

## 6 FUTURE WORK

This work examines a new source of side-channel information leakage from a victim workload arising due to the conversion of data-dependent power consumption to data-dependent execution time. Future work falls along the following non-orthogonal vectors:

- **Other channels:** Extending the analysis to other data-dependent reactive limits, such as thermal limits, not covered by the present case study. Such channels may yield differing SNR. As a general rule, internally sampled telemetry tends to increase in fidelity over time, suggesting future products require extra care.
- **Other victims:** Extending the analysis to other cryptographic primitives (e.g., asymmetric primitives such as EcDSA [1]) and cryptographic applications susceptible to power side channels.
- **Using stressor code:** This paper focused on reducing reactive limits as a primary means to trigger frequency throttling. As stated before, an alternative option is running a stressor workload, which should consume high but constant power, to boost power or current consumption. Investigating this complementary option is part of future work.
- **Improved data analysis methodologies:** While TVLA is a well recognized approach to detecting statistically significant variation in power traces, other techniques have been proposed that may serve to refine the work (e.g., NICV [12], HAC [2]). An investigation of ML-based data analysis methods and comparison with CPTA may prove fruitful.
- **Improved mitigation strategies:** The growing intersection between the fields of security and power management warrants better trade-offs between security and system power, performance and responsiveness—ideally, allowing all goals to be simultaneously met. We may consider designs with better power infrastructure virtualization, isolation or control.

## 7 CONCLUSION

In this paper, we present a novel frequency throttling side-channel analysis attack against constant-cycle software cryptographic implementations. The root cause of such a side-channel is a power side-channel, which is converted to a timing side-channel by the power management architecture. We demonstrate the threat posed by frequency throttling side-channel attacks by considering a constant-cycle implementation of AES encryption as a case study. The outcomes of our experimental evaluations highlight the effectiveness of frequency throttling side-channel analysis to retrieve the secret AES key, by applying the CPTA technique on the collected timing traces. Finally, we present a set of options to thwart such throttling side-channel analysis attacks, with analysis of pros and cons. These mitigation options provide insights into the necessary conditions for throttling side-channel information leakage and how to develop effective countermeasures.

## REFERENCES

- [1] Monjur Alam, Baki Yilmaz, Frank Werner, Niels Samwel, Alenka Zajic, Daniel Genkin, Yuval Yarom, and Milos Prvulovic. 2021. Nonce@Once: A Single-Trace EM Side Channel Attack on Several Constant-Time Elliptic Curve Implementations in Mobile Platforms. In *2021 IEEE European Symposium on Security and Privacy (EuroS P)*. 507–522. <https://doi.org/10.1109/EuroSP51992.2021.00041>
- [2] Alric Althoff, Jeremy Blackstone, and Ryan Kastner. 2019. Holistic Power Side-Channel Leakage Assessment: Towards a Robust Multidimensional Metric. In *2019 IEEE/ACM International Conference on Computer-Aided Design (ICCAD)*. 1–8. <https://doi.org/10.1109/ICCAD45719.2019.8942098>
- [3] AMD. 2014. Ryzen\_Monitor. [https://github.com/hattedsquiritel/ryzen\\_monitor](https://github.com/hattedsquiritel/ryzen_monitor). (2014). Accessed: 2022-05-01.
- [4] AMD. 2018. BIOS and Kernel Developer’s Guide (BKDG) for AMD Family 15h Models 70h-7Fh Processors. [https://www.amd.com/system/files/TechDocs/55072\\_AMD\\_Family\\_15h\\_Models\\_70h-7Fh\\_BKDG.pdf](https://www.amd.com/system/files/TechDocs/55072_AMD_Family_15h_Models_70h-7Fh_BKDG.pdf). (2018). Accessed: 2022-05-01.
- [5] AMD. 2022. AMD CVE-2020-12912. <https://nvd.nist.gov/vuln/detail/CVE-2020-12912>. (2022). Accessed: 2022-04-12.
- [6] AMD. 2022. AMD Ryzen Technology: Precision Boost 2 Performance Enhancement. <https://www.amd.com/en/support/kb/faq/cpu-pb2>. (2022). Accessed: 2022-03-12.
- [7] AMD. 2022. AMD uProf User Guide. [https://developer.amd.com/wordpress/media/2013/12/User\\_Guide.pdf](https://developer.amd.com/wordpress/media/2013/12/User_Guide.pdf). (2022). Accessed: 2022-4-21.
- [8] AMD. 2022. Ryzen Master 2.9 - Reference Guide. <https://www.amd.com/system/files/documents/ryzen-master-quick-reference-guide.pdf>. (2022). Accessed: 2022-05-01.
- [9] ARM. 2022. ARMv8-A Power Management. <https://developer.arm.com/documentation/100960/0100/ARMv8-A-Power-management?lang=en>. (2022). Accessed: 2022-04-10.
- [10] Karl Johan Åström and Richard M Murray. 2010. Feedback systems. In *Feedback Systems*. Princeton university press.
- [11] Grant Ayers, Nayana Prasad Nagendra, David I. August, Hyouon Kyu Cho, Svilen Kanev, Christos Kozyrakis, Trivikram Krishnamurthy, Heiner Litz, Tipp Moseley, and Parthasarathy Ranganathan. 2019. AsmDB: Understanding and Mitigating Front-End Stalls in Warehouse-Scale Computers. In *International Symposium on Computer Architecture (ISCA)*.
- [12] Shivam Bhasin, Jean-Luc Danger, Sylvain Guilley, and Zakaria Najm. 2014. NICV: Normalized inter-class variance for detection of side-channel leakage. In *2014 International Symposium on Electromagnetic Compatibility, Tokyo*. 310–313.
- [13] W Lloyd Bircher and Lizy K John. 2008. Analysis of dynamic power management on multi-core processors. In *Proceedings of the 22nd annual international conference on Supercomputing*. 327–338.
- [14] Eric Brier, Christophe Clavier, and Francis Olivier. 2004. Correlation Power Analysis with a Leakage Model. In *Cryptographic Hardware and Embedded Systems - CHES 2004*, Marc Joye and Jean-Jacques Quisquater (Eds.). Springer Berlin Heidelberg, Berlin, Heidelberg, 16–29.
- [15] Maxime Colmant, Pascal Felber, Romain Rouvoy, and Lionel Seinturier. 2017. WattsKit: Software-Defined Power Monitoring of Distributed Systems. *2017 17th IEEE/ACM International Symposium on Cluster, Cloud and Grid Computing (CCGRID)* (2017), 514–523.
- [16] Compaq Computer Corporation and Revision B. 2000. Advanced Configuration and Power Interface Specification. (2000). <http://www.acpi.info/>
- [17] Victor Costan and Srinivas Devadas. 2016. Intel SGX explained. *Cryptology ePrint Archive* (2016).
- [18] Guillaume Fieni, Romain Rouvoy, and Lionel Seinturier. 2020. SmartWatts: Self-Calibrating Software-Defined Power Meter for Containers. *2020 20th IEEE/ACM International Symposium on Cluster, Cloud and Internet Computing (CCGRID)* (2020), 479–488.
- [19] Matteo Maria Fusi. 2016. *Information-Leakage Analysis based on Hardware Performance Counters*. Master’s thesis. The Polytechnic University of Milan.
- [20] Benjamin Jun Gilbert Goodwill, Josh Jaffe, Pankaj Rohatgi, et al. 2011. A testing methodology for side-channel resistance validation. In *NIST non-invasive attack testing workshop*, Vol. 7.
- [21] Gilbert Goodwill, Benjamin Jun, Josh Jaffe, and Pankaj Rohatgi. 2011. P.: A testing methodology for side-channel resistance validation, NIAT. (2011).
- [22] Corey Gough, Ian Steiner, and Winston Saunders. 2015. CPU power management. In *Energy Efficient Servers*. Springer, 21–70.
- [23] Shay Gueron. 2010. Intel® Advanced Encryption Standard (AES) New Instructions Set. (2010).
- [24] Jawad Haj-Yahya, Avi Mendelson, Yosi Ben-asher, and Anupam Chattopadhyay. 2018. *Energy Efficient High Performance Processors Recent Approaches for Designing Green High Performance Computing*. <https://doi.org/10.1007/978-981-10-8554-3>
- [25] J. Haj-Yahya, L. Orosa, J. S. Kim, J. Gomez Luna, A. Yaglikci, M. Alser, I. Puddu, and O. Mutlu. 2021. IChannels: Exploiting Current Management Mechanisms to Create Covert Channels in Modern Processors. In *2021 ACM/IEEE 48th Annual International Symposium on Computer Architecture (ISCA)*. IEEE Computer Society, Los Alamitos, CA, USA, 985–998. <https://doi.org/10.1109/ISCA52012.2021.00081>
- [26] Peter H. Hochschild, Paul Jack Turner, Jeffrey C. Mogul, Rama Krishna Govindaraju, Parthasarathy Ranganathan, David E Culler, and Amin Vahdat. 2021. Cores that don’t count. In *Proc. 18th Workshop on Hot Topics in Operating Systems (HotOS 2021)*.
- [27] Intel. 2022. Guidelines for Mitigating Timing Side Channels Against Cryptographic Implementations. <https://www.intel.com/content/www/us/en/developer/articles/technical/software-security-guidance/secure-coding/mitigate-timing-side-channel-crypto-implementation.html>. (2022). Accessed: 2022-05-02.
- [28] Intel. 2022. Intel CVE-2020-8694. <https://www.intel.com/content/www/us/en/security-center/advisory/intel-sa-00389.html>. (2022). Accessed: 2022-04-12.
- [29] Intel. 2022. Intel Running Average Power Limit Energy Reporting. <https://www.intel.com/content/www/us/en/developer/articles/technical/software-security-guidance/advisory-guidance/running-average-power-limit-energy-reporting.html>. (2022). Accessed: 2022-04-12.
- [30] Intel. 2022. Intel SGX. <https://software.intel.com/en-us/sgx>. (2022). Accessed: 2022-05-02.
- [31] Intel. 2022. Intel® 64 and IA-32 Architectures Software Developer Manuals. <https://software.intel.com/content/www/us/en/develop/articles/intel-sdm.html>. (2022). Accessed: 2022-05-02.
- [32] Intel. 2022. Intel® Integrated Performance Primitives Cryptography. <https://github.com/intel/ipp-crypto>. (2022). Accessed: 2022-04-07.
- [33] Intel. 2022. Overview of Enhanced Intel SpeedStep® Technology for Intel® Processors. <https://www.intel.com/content/www/us/en/support/articles/000007073/processors.html>. (2022). Accessed: 2022-04-07.
- [34] Intel. 2022. Overview of Intel® Speed Shift Technology. <https://edc.intel.com/content/www/us/en/design/ipla/software-development-platforms/client/platforms/alder-lake-desktop/12th-generation-intel-core-processors-datashet-volume-1-of-2/002/intel-speed-shift-technology/>. (2022). Accessed: 2022-04-07.
- [35] David Kaplan, Jeremy Powell, and Tom Woller. 2016. AMD memory encryption. (2016).
- [36] Wonyoung Kim, Meeta S Gupta, Gu-Yeon Wei, and David Brooks. 2008. System level analysis of fast, per-core DVFS using on-chip switching regulators. In *2008 IEEE 14th International Symposium on High Performance Computer Architecture*. IEEE, 123–134.
- [37] Paul Kocher, Joshua Jaffe, Benjamin Jun, and Pankaj Rohatgi. 2011. Introduction to differential power analysis. *Journal of Cryptographic Engineering* 1, 1 (2011), 5–27.
- [38] Andreas Kogler, Daniel Gruss, and Michael Schwarz. 2022. Minefield: A Software-only Protection for SGX Enclaves against DVFS Attacks. In *USENIX Security Symposium*.
- [39] leogx9r. 2022. Ryzen SMU. [https://gitlab.com/leogx9r/ryzen\\_smu](https://gitlab.com/leogx9r/ryzen_smu). (2022).
- [40] Moritz Lipp, Andreas Kogler, David Oswald, Michael Schwarz, Catherine Eason, Claudio Canella, and Daniel Gruss. 2021. PLATYPUS: Software-based Power Side-Channel Attacks on x86. In *2021 IEEE Symposium on Security and Privacy (SP)*. 355–371.
- [41] Chen Liu, Monodeep Kar, Xueyang Wang, Nikhil Chawla, Neer Roggel, Bilgiday Yuce, and Jason M Fung. 2021. Methodology of Assessing Information Leakage through Software-Accessible Telemetries. In *2021 IEEE International Symposium on Hardware Oriented Security and Trust (HOST)*. IEEE, 259–269.
- [42] Stefan Mangard, Elisabeth Oswald, and Thomas Popp. 2008. *Power analysis attacks: Revealing the secrets of smart cards*. Vol. 31. Springer Science & Business



- Media.
- [43] Heiko Mantel, Johannes Schickel, Alexandra Weber, and Friedrich Weber. 2018. How secure is green IT? The case of software-based energy side channels. In *ESORICS*. Springer.
- [44] Microsoft. 2022. rdtsc instruction. <https://docs.microsoft.com/en-us/cpp/intrinsics/rdtsc?view=msvc-170>. (2022). Accessed: 2022-04-11.
- [45] Mathias Morbitzer, Sergej Proskurin, Martin Radev, Marko Dorfhuber, and Erick Quintanar Salas. 2021. SEVerity: Code Injection Attacks against Encrypted Virtual Machines. In *2021 IEEE Security and Privacy Workshops (SPW)*. 444–455. <https://doi.org/10.1109/SPW53761.2021.00063>
- [46] Rajeev Muralidhar, Renata Borovica-Gajic, and Rajkumar Buyya. 2022. Energy Efficient Computing Systems: Architectures, Abstractions and Modeling to Techniques and Standards. *ACM Comput. Surv.* (jan 2022). <https://doi.org/10.1145/3511094> Just Accepted.
- [47] Adel Nouredine, Romain Rouvoy, and Lionel Seinturier. 2015. Monitoring Energy Hotspots in Software. *Automated Software Engg.* 22, 3 (sep 2015), 291–332. <https://doi.org/10.1007/s10515-014-0171-1>
- [48] National Institute of Standards and Technology. 2001. *ADVANCED ENCRYPTION STANDARD (AES)*. Technical Report. U.S. Department of Commerce, Washington, D.C.
- [49] Emmanuel Prouff and Matthieu Rivain. 2013. Masking against Side-Channel Attacks: A Formal Security Proof. In *2013 Annual International Conference on the Theory and Applications of Cryptographic Techniques (EUROCRYPT '13)*.
- [50] Matthieu Rivain. 2009. *Selected Areas in Cryptography: 15th International Workshop, SAC 2008, Sackville, New Brunswick, Canada, August 14-15, Revised Selected Papers*. Chapter On the Exact Success Rate of Side Channel Analysis in the Gaussian Model, 165–183.
- [51] Efraim Rotem, Alon Naveh, Avinash Ananthkrishnan, Eliezer Weissmann, and Doron Rajwan. 2012. Power-Management Architecture of the Intel Microarchitecture Code-Named Sandy Bridge. *IEEE Micro* 32, 2 (2012), 20–27. <https://doi.org/10.1109/MM.2012.12>
- [52] Tobias Schneider and Amir Moradi. 2015. Leakage Assessment Methodology. In *Cryptographic Hardware and Embedded Systems – CHES 2015*. Tim Güneysu and Helena Handschuh (Eds.). Springer Berlin Heidelberg, Berlin, Heidelberg, 495–513.
- [53] Brijesh Singh. 2017. x86: Secure Encrypted Virtualization (AMD). (2017).
- [54] François-Xavier Standaert. 2017. How (not) to Use Welch’s T-test in Side-Channel Security Evaluations. In *IACR Cryptol. ePrint Arch.*
- [55] Lin Yan, Yao Guo, Xiangqun Chen, and Hong Mei. 2015. A Study on Power Side Channels on Mobile Devices. In *Proceedings of the 7th Asia-Pacific Symposium on Internetware*. 30–38.

## A APPENDIX

We examined the applicability of a frequency throttling side-channel attack to an AMD processor. We consider the same AES-NI-based implementation of an AES-128 victim workload and demonstrate PoC results on a Ryzen 7 5600G processor (codename "Cezanne").

### A.1 Reactive Limits on Ryzen 7

The reactive limits supported by the Ryzen processor include:

- Package Power Tracking (PPT): the total power capacity in Watts at the processor socket, including memory controller power for a CPU [8].
- Package Power Tracking (PPT) Fast: PPT limit with faster response time.
- Thermal Design Current (TDC): the total current capacity in Amperes at the thermal throttling limit of the processor [8].

The System Management Unit (SMU) is a sub-component of the AMD processor that is responsible for a variety of system and power management tasks during boot and runtime [4]. The aforementioned reactive limits can be configured from system software via an SMU mailbox interface with support from a kernel driver [3, 39].

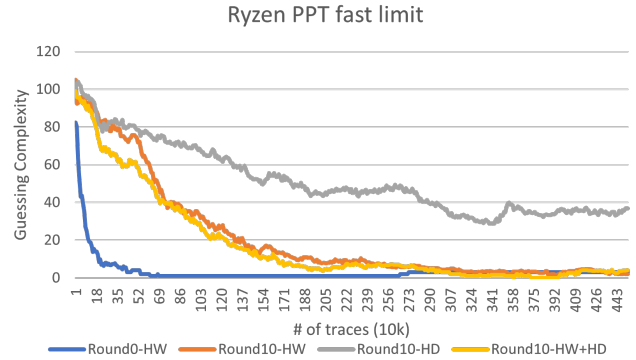


**Figure 6: Guessing Complexity trend with different amounts of traces on an AMD Ryzen 7 5600G processor, with PPT fast limit induced frequency throttling**

### A.2 CPTA results with PPT Fast Limit

We followed the attack methodology comprising of offline, online and analysis phases detailed in section 4.2, to mount a CPTA attack. In the offline phase, the attacker sets PPT Fast Limit to 15W to trigger frequency throttling. In the online phase, the attacker inputs plaintexts to a victim workload and collects ciphertexts and timing traces ( $T_\delta$ ). The victim workload is executed on 6 available physical cores and each encryption with the same plaintext and key is repeated, such that  $T_\delta$  is around 50ms for every trace. We collected 4.5M traces with trace collection time of 63 hours. In the analysis phase, we considered the same points of attack, generated execution time estimates ( $T_h^k$ ) and computed GC as described earlier in section 4.2.3.

Figure 6 shows the trend in GC against the number of traces collected for CPTA analysis, for different execution time estimate models. The GC converges much faster with Round0-HW model as compared to other execution time estimate models. GC reduces to near 0 with less than 1 million traces with Round-0 HW model, indicating most bytes of the secret key are revealed in less than 16 hours. A similar trend in GC is observed with Round10-HW and Round10-HW+HD models, with GC converging to 0 with approximately 3 million traces. GC converges slowest with Round10-HD model (GC=40 with 4.5 million traces). In summary, this observation confirms the frequency throttling side-channel on an AMD Ryzen processor.